Mesoscale fluid-particle interaction using two-way coupled SPH and the Discrete Element Method

Martin Robinson
Multiscale Mechanics
University of Twente
Enschede, Netherlands
m.j.robinson@ctw.utwente.nl

Marco Ramaioli
Nestle Research Center
Lausanne, Switzerland
Marco.Ramaioli@rdls.nestle.com

***Abstract*—We present a meshless simulation method for multiphase fluid-particle systems using Smoothed Particle Hydrodynamics (SPH) and the Discrete Element Method (DEM). Rather than fully resolving the interstitial fluid, which is often infeasible, we use an unresolved fluid model based on the locally averaged Navier Stokes equations. A variable-h SPH formulation is used to calculate the fluid phase, where the density of each particle is proportional to the local porosity. The SPH-DEM method is validated using simulations of single and multiple particle sedimentation in a 3D water column. The velocity and terminal velocity for the single particle compares well with the analytical solution, provided that the minimum resolution of the fluid phase is much larger than the solid particle diameter. In the multiple particle sedimentation simulation, the two-way coupling between the phases permits the growth of a Rayleigh-Taylor instability. The growth rate of the instability in the linear regime is calculated and compares well with theory.**

I. Introduction

Fluid-particle systems are ubiquitous in nature and industry. Sediment transport and erosion are important in many environmental studies and the interaction between particles and interstitial fluid affects the rheology of avalanches, slurry flows and soils. In industry, the efficiency of a fluidised bed process (e.g. Fluidized Catalytic Cracking) is completely determined by the complex two-way interaction between the injected gas flow and the solid granular material. The dispersion of solid particles in a fluid is also of broad industrial relevance in the food, chemical and painting industries.

The length-scale of interest determines the method of simulation for fluid-particle systems. For very small scale processes it is feasible to fully resolve the interstitial fluid between the particles (see [1]–[3] for a few examples of particle or pore-scale SPH simulations). However, for many applications the dynamics of interest occur over length scales much greater than the particle diameter and it becomes necessary to use unresolved, or mesoscale, fluid simulations.

Fluid-particle simulations at this scale are often given the term Discrete Particle Models (DPM). These models fully resolve the individual particles using a Lagrangian model for the solid phase. The fluid phase does not resolve the interstitial fluid, but instead models the locally averaged Navier-Stokes equations and is coupled to the solid particles using appropriate drag closures. Most of the prior work on DPMs have been done using grid-based methods for the fluid phase, and a few relevant examples can be seen in the papers by Tsuiji et al. [4], Xu [5], [6] or Hoomans et al. [7], [8].

Fixed pore flow simulations using SPH for the (unresolved) fluid phase have been described by Li et al. [9] and Jiang et al. [10], but these do not allow for the motion and collision of solid grains. Cleary et al. [11] and Fernandez et al. [12] simulate slurry flow at the mesoscale using SPH and DEM in SAG mills and through industrial banana screens, but only perform a one-way coupling between the solid and fluid phases.

The SPH-DEM model presented in this paper can be used for both one and two-way coupling and is suitable for both dilute and dense particle systems. It is based on the locally averaged Navier-Stokes (AVNS) equations that were first derived by Anderson and Jackson in the sixties [13], and have been used with great success to model the complex fluid-particle interactions occurring in industrial fluidized beds [14]. Anderson and Jackson defined a smoothing operator identical to that used in SPH and used it to reformulate the NS equations in terms of smoothed variables and a local porosity field (porosity refers to the fraction of fluid in a given volume). Given its theoretical basis in kernel interpolation, it is natural to consider the use of the SPH method to solve the AVNS equations, coupled with a DEM model for the solid phase. This results in a purely particle-based solution method and therefore enjoys the flexibility that is inherent in these methods. In particular, the SPH-DEM model described in this paper is well suited for applications involving a free surface, including (but not limited to) debris flows, avalanches, landslides, sediment transport or erosion in rivers and beaches, slurry transport in industrial processes (e.g. SAG mills) and liquid-powder mixing in the food processing industry.

Sections II-IV describes the AVNS equations and the SPH and DEM models for the fluid and solid phases. The remainder of the paper then describes SPH-DEM simulations of single (Section V) and multiple (Section VI) particle sedimentation in a 3D water column. These results are compared against analytical solutions in order to validate the proposed model.

II. The Locally Averaged Navier-Stokes Equations

Most models of the unresolved fluid phase are based on the locally averaged Navier-Stokes equations derived by Anderson and Jackson [13]. Anderson and Jackson defined a local averaging based on a radial smoothing function $g(r)$ with similar properties to the SPH kernel. The function $g(r)$ is greater than zero for all r and decreases monotonically with increasing r, it possesses derivatives $g^n(r)$ of all orders and is normalised so that

$$\int g(r)dV = 1 \tag{1}$$

The local average of any fluid variable $a'(x)$ can be obtained by convolution with the smoothing function

$$\epsilon(x)a(x) = \int_{V_f} a'(y)g(x-y)dV_y, \tag{2}$$

where x and y are position coordinates which are one dimensional for simplicity. The integral is taken over the volume of interstitial fluid and $\epsilon(x)$ is the porosity.

$$\epsilon(x) = 1 - \int_{V_s} g(x-y)dV_y, \tag{3}$$

where the integral is taken over the volume of the solid particles.

Applying this averaging method to the Navier-Stokes equations, Anderson and Jackson derived the following continuity equation in terms of locally averaged variables

$$\frac{\partial(\epsilon\rho)}{\partial t} + \nabla\cdot(\epsilon\rho\mathbf{u}) = 0, \tag{4}$$

where ρ is the fluid mass density and $\mathbf{u}$ is the fluid velocity. The corresponding momentum equation is

$$\rho\epsilon\left(\frac{\partial\mathbf{u}}{\partial t} + \mathbf{u}\cdot\nabla\mathbf{u}\right) = -\nabla P + \nabla\cdot\boldsymbol{\tau} - n\mathbf{f} + \epsilon\rho\mathbf{g}, \tag{5}$$

where P is the fluid pressure, $\boldsymbol{\tau}$ is the viscous stress tensor and $n\mathbf{f}$ is the fluid-particle coupling term. The coefficient for the coupling term n is the local average of the number of particles per unit volume and $\mathbf{f}$ is the local mean value of the force exerted on the particles by the fluid.

The force on each solid particle by the fluid is

$$\mathbf{f} = V_p(-\nabla P + \nabla\cdot\boldsymbol{\tau}) + \mathbf{f}^d, \tag{6}$$

where the first and second terms model the effect of the resolved fluid forces on the particle and $\mathbf{f}^d$ is a particle drag force. This force depends on the unresolved fluctuations in the fluid variables and is normally defined using both theoretical arguments and fits to experimental data. For a single particle in 3D creeping flow this term would simply be the Stokes drag force. For higher Reynolds numbers and multiple particle interactions this term is determined using fits to numerical or experimental data [15].

III. SPH implementation of the AVNS equations

SPH is based on an identical local averaging technique to that used in the AVNS equations, so it is natural to convert the interpolation integrals in Eqs. 2 and 3 to SPH sums using a smoothing kernel $W(x,h)$ in place of $g(r)$. Therefore the calculation of an arbitrary variable $a(x)$ becomes

$$\epsilon(x)a(x) = \sum_b a'(r_b)W(x-r_b,h)\frac{m_b}{\rho_b}, \tag{7}$$

where the sum is over all SPH particles within $2h$ of x and r_b, m_b and ρ_b are the position, mass and density of SPH particle b.

To calculate the porosity ϵ_a at SPH particle a, the integral in (3) is converted into a sum over all DEM particles within the kernel radius and becomes

$$\epsilon_a = 1 - \sum_j W(r_a - r_p, h_a)V_j, \tag{8}$$

where V_j is the volume of DEM particle j. For readability, sums over SPH particles use the subscript b, while sums over surrounding DEM particles use the subscript j.

Applying the local averaging method to the Navier-Stokes equations, Anderson and Jackson derived the continuity and momentum equations shown in Eq. 4 and 5 respectively. To convert these to SPH equations we first define a superficial density $\overline{\rho}_a$ for SPH particle a

$$\overline{\rho}_a = \epsilon_a\rho_a = \sum_b m_b W_{ab}, \tag{9}$$

where $W_{ab} = W(r_a - r_b, h)$.

Substituting the superficial density into the averaged continuity and momentum equations reduces them to the normal Navier-Stokes equations. Therefore, our approach is to use the standard compressible SPH equations using the superficial density $\overline{\rho}$ in place of the density and adding terms to model the fluid-particle drag.

Neglecting gravity, the SPH acceleration equation becomes

$$\frac{d\mathbf{u}_a}{dt} = -\sum_b m_b\left(\frac{P_b}{\overline{\rho}_b^2} + \frac{P_b}{\overline{\rho}_b^2} + \Pi_{ab}\right)\nabla_a W_{ab} + \mathbf{f}_a/m_a, \tag{10}$$

where $\mathbf{f}_a$ is the coupling force on the SPH particle a due to the DEM particles. The pressure is calculated using the weakly compressible equation of state, but with the reference density scaled by the local porosity

$$P_a = B_a\left(\left(\frac{\overline{\rho}_a}{\epsilon_a\rho_0}\right)^\gamma - 1\right). \tag{11}$$

The scaling factor B_a is set so that the variation from the new reference density is less than 1 percent

$$B_a = \frac{100\epsilon_a\rho_0 v_m^2}{\gamma}, \tag{12}$$

where v_m is the maximum velocity of the fluid.

As the superficial density will vary according to the local porosity, care must be taken to update the smoothing length for all particles in order to maintain a sufficient number of neighbour particles. The smoothing length h_a is calculated using

$$h_a = \sigma \left(\frac{m_a}{\overline{\rho}_a} \right)^{1/d}, \tag{13}$$

where d is the number of dimensions and σ determines the resolution of the summation interpolant. The value used in all the simulation results presented here is $\sigma = 1.5$.

The most obvious effect of allowing the density and smoothing length to vary according to the porosity is that the resolution of the method will reduced in areas of high porosity. The smoothing length h is proportional to $h \propto (1/\epsilon)^{1/d}$. Compare this with the Einstein's [16] equation for effective viscosity for a dilute suspensions

$$\mu_{eff} = \mu[1 + 2.5(1 - \epsilon)], \tag{14}$$

or the effective viscosity by Krieger [17] using a hard sphere model

$$\frac{\mu_c}{\mu_f} = \left(\frac{\epsilon - \epsilon_{min}}{1 - \epsilon_{min}} \right)^{-2.5(1-\epsilon_{min})}, \tag{15}$$

where $\epsilon_{min} = 0.37$ is the porosity at the maximum packing of the solid particles.

Keeping in mind that the Reynolds number is inversely proportional to the viscosity, it can be seen that for both of these equations and for all dimensions greater than 1, the effective Reynolds number decreases more quickly than the SPH resolution. Therefore, not only is the variable-h SPH formulation presented valid for a wide range of porosities, it is also computationally efficient thanks to the natural variation in resolution with effective Reynolds number.

The SPH viscosity term Π_{ab} is unchanged and is calculated using the term proposed by Monaghan [18].

IV. Discrete Element Model (DEM)

In DEM (also known as Molecular Dynamics), Newton's equations of motion are integrated for each individual solid particle. Interactions between the particles are explicit force expressions that are used whenever two particles come into contact.

Given a DEM particle i with position r_i, the equation of motion is

$$m_i \frac{d^2 r_i}{dt^2} = \sum_j \mathbf{c}_{ij} + \mathbf{f}_i + m_i \mathbf{g}, \tag{16}$$

where m_i is the mass of particle i, $\mathbf{c}_{ij}$ is the contact force between particles i and j and $\mathbf{f}_i$ is the fluid-particle coupling term. For the simulations presented below, we have used the linear spring dashpot contact model

$$\mathbf{c}^{ij} = -(k\delta - \beta\dot{\delta})\mathbf{n}_{ij}, \tag{17}$$

where δ is the overlap between the two particles and $\mathbf{n}_{ij}$ is the unit normal vector pointing from j to i. $k = 2.5 \times 10^5 kg/s^2$ and $\beta = 2.0 kg/s$ is the spring and damping constant respectively. The simulation timestep is calculated based on a typical contact duration and is given by

$$\Delta t = \frac{\pi}{50\omega}, \tag{18}$$

$$\omega = \sqrt{(2k/m_i) - \beta/m_i}. \tag{19}$$

This timestep is significantly smaller than the normal SPH CFL condition and in most cases sets the minimum timestep for the SPH-DEM method.

Anderson and Jackson [13] give the force on particle i due to the fluid as

$$\mathbf{f}_i = V_i(-\nabla P + \nabla \cdot \tau) + \mathbf{f}_d(\epsilon_i, \mathbf{u}_s), \tag{20}$$

where the pressure and stress tensor are the local values of the fluid variables. The pressure gradient and the divergence of the stress tensor are evaluated at each solid particle using a Shepard corrected [19] SPH interpolation. Rather than interpolating either P or τ and then finding the gradients, the pressure gradient and viscous force fields calculated at each SPH particle are interpolated directly to each DEM particle.

The drag force $\mathbf{f}_d$ depends on the relative velocity between the two phases, otherwise known as the superficial velocity. If $\mathbf{u}_f$ and $\mathbf{u}_i$ are the fluid and particle velocity respectively, then the superficial velocity is defined as $\mathbf{u}_s = \epsilon(\mathbf{u}_f - \mathbf{u}_i)$. Once again, the fluid velocity $\mathbf{u}_f$ is found at each DEM particle using a Shepard corrected SPH interpolation.

The simplest drag law is Stokes drag, which is valid for a single particle in creeping flow and is defined as

$$\mathbf{f}_d = 3\pi\mu d\mathbf{u}_s, \tag{21}$$

where d is the particle diameter.

For higher Reynolds numbers and multiple particles, the drag law can be generalised to

$$\mathbf{f}_d = \frac{1}{8} C_d f(\epsilon) \pi d^2 \rho |\mathbf{u}_s| \mathbf{u}_s, \tag{22}$$

where C_d is a drag coefficient that varies with the particle Reynolds number $Re_p = \rho \mathbf{u}_s d/\mu$, and $f(\epsilon)$ is the voidage function that models the interactions between multiple particles in the fluid.

A popular definition for the drag coefficient was proposed by Dallavalle [20]

$$C_d = \left[0.63 + \frac{4.8}{\sqrt{Re_p}} \right]. \tag{23}$$

Di Felice proposed a voidage function based on experimental data of fluid flow through packed spheres [21]

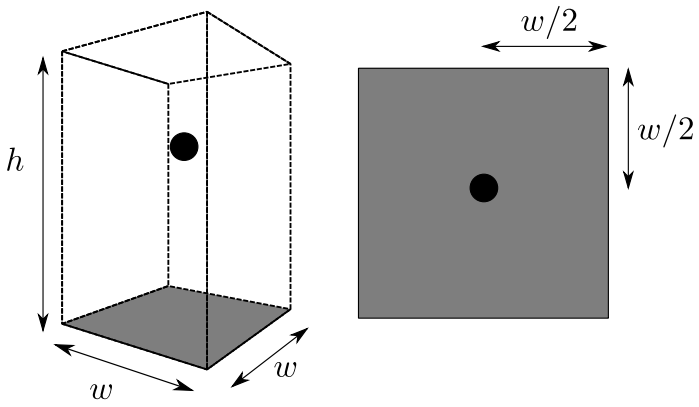

Fig. 1. Setup for single particle sedimentation test

$$f(\epsilon) = \epsilon^{-\xi}, \tag{24}$$

$$\xi = 3.7 - 0.65 \exp\left[-\frac{(1.5 - \log_{10} Re_p)^2}{2}\right]. \tag{25}$$

Both the Stokes drag term and the combination of Dallavalle and Di Felice's drag terms are used in the simulations presented in this paper.

In order to satisfy Newtons third law, the fluid-particle coupling force on the fluid must be equal and opposite to the force on the solid particles. Each DEM particle is contained within multiple SPH interaction radii, so care must be taken to ensure that the two coupling forces are balanced.

The coupling force on SPH particle a is determined by interpolating the fluid-particle coupling force on the surrounding DEM particles

$$\mathbf{f}_a = -\frac{m_a}{\rho_a} \sum_j \frac{1}{S_j} \mathbf{f}_j W_{aj}. \tag{26}$$

The scaling factor S_j is added to ensure that the force on the fluid phase exactly balances the force on the solid particles. It is given by

$$S_i = \sum_b \frac{m_b}{\rho_b} W_{ib}, \tag{27}$$

where the sum is taken over all the SPH particles surrounding DEM particle i. For a DEM particle immersed in the fluid this will be close to unity.

V. Single Particle Sedimentation

In order to validate the SPH-DEM model we have used several 3D test cases involving sedimenting particles in a water column. This section describes the first test case, that of a single sedimenting particle. Figure 1 shows the geometry. The water column has a height of $h = 1.5$ and the bottom boundary is constructed using lennard-jones repulsive particles (these particles are identical to those used by Monaghan et al. in [22]). The boundaries in the x and y directions are periodic with a width of $w = 1$ and gravity acts in the negative z direction. The single DEM particle is initialised at $z = 0.75$. It has a diameter equal to $d = w/20$ and has a density 8 times greater than the surrounding fluid ($\rho = 1000$). The dynamic viscosity of the fluid is set to $\nu = 0.0218$, which results in a particle Reynolds number of $Re_p = 1$.

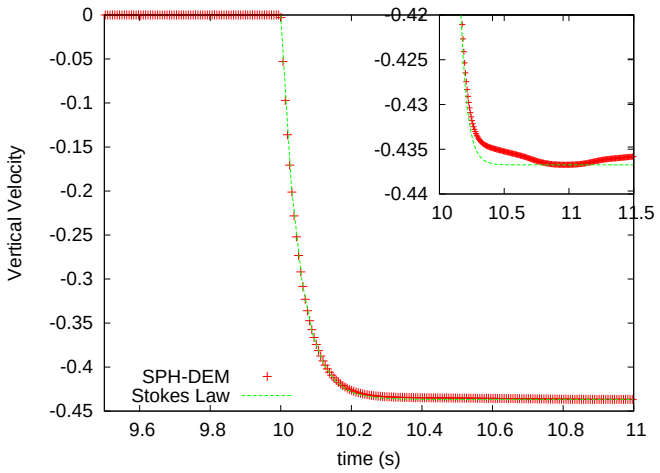

Fig. 2. Sedimentation velocity for single particle with one-way coupling compared with the analytical solution derived from Stokes drag. The inset shows the same plot zoomed in to show the exact steady state terminal velocity.

For the first 10 s of the simulation, the position of the DEM particle is fixed and the fluid is allowed to reach hydrostatic equilibrium. The particle is then released and allowed to fall under gravity at $t = 10s$.

The standard Stokes law (see Eq. 21) is used to calculate the drag force on the particle. Since Stokes drag law assumes a quiescent fluid, the force on the fluid due to the particle is initially set to zero (this implements a one-way coupling between the phases). Subsequent results will explore the effect of a two-way coupling.

Figure 2 show the evolution of the DEM particle's vertical velocity using the one-way coupling. Also shown is the expected analytical velocity given by

$$v(t) = \frac{(\rho_s - \rho)Vg}{b}\left(1 - e^{-bt/m}\right), \tag{28}$$

$$b = 3\pi\mu d, \tag{29}$$

where ρ_s is the solid particle density.

The vertical velocity of the falling DEM particles matches the analytical velocity very well, with no discernible difference between the data and the analytical expression. The plot inset in Figure 2 shows a zoomed portion of the main plot, which reveals that the final terminal velocity of the particle is within 2% of the expected value.

However, one of the main goals of the SPH-DEM formulation described in this paper is to simulate the two-way coupling between the particle and fluid phases, and therefore it is instructive to consider the effect on the single sedimenting particle when the full two-way coupling is used. Figure 3

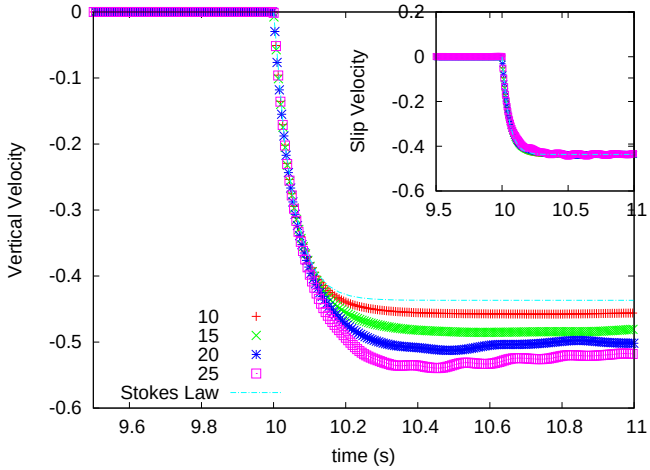

Fig. 3. Sedimentation velocity for single particle with two-way coupling at various resolutions. The resolution number indicates the number of fluid particles across the box width w. The inset shows the superficial, or slip, velocity versus time.

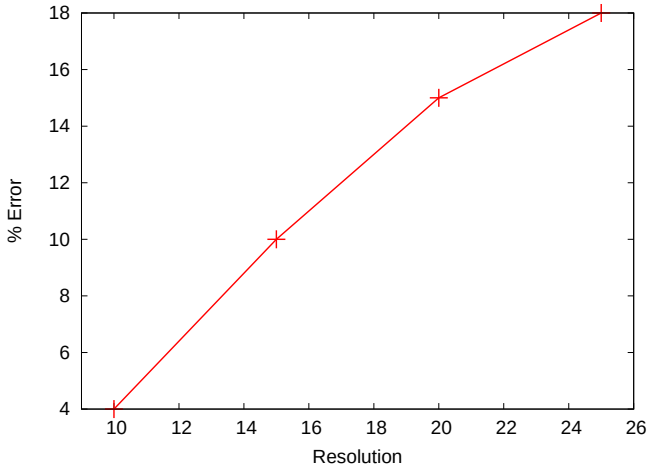

Fig. 4. Percentage error in the terminal velocity (as compared with Stokes drag analytical solution) for different fluid resolutions.

shows the vertical velocity data for multiple simulation runs using different numbers of SPH particles for the fluid, ranging from 10x10x15 particles (the lowest resolution, which is also the resolution used for the previous results in Figure 2) to 25x25x37. The general trend shown in these plots is that the sedimentation velocity of the DEM particle increases for higher resolutions. This effect is due to the increase of the fluid's vertical velocity in the region directly surrounding the particle. This is confirmed by the plot inset, which shows the particle's slip velocity (ie. the superficial velocity $\mathbf{u}_s = \epsilon(\mathbf{u}_f - \mathbf{u}_i)$) versus time for all the different runs. As can be seen, these plots all collapse onto the one line, confirming that it is the fluid velocity in the region of the DEM particle that results in the higher terminal velocities.

Due to the two-way coupling, the drag force on the particle will be felt by the fluid as an equal and opposite force. This will accelerate the particles by a amount proportional to the mass of the SPH particles. For higher resolutions the mass of the SPH particles is lower, leading to an increase in vertical velocity of the affected fluid particles. Since the DEM particle's drag force depends on the velocity difference between the phases, this will lead to a increase in the particle's terminal velocity. Figure 4 shows the error in the terminal velocity of the DEM particle versus the resolution used. As can be seen, the change in the terminal velocity for the higher resolutions is significant and in the range of 10-20% for SPH particle separations of $1.25d$ - $0.75d$, where d is the diameter of the DEM particle.

While unexpected at first, this result can be explained by examining the limitations of the AVNS equations that are used for the fluid phase. The AVNS equations assume that the width of the smoothing kernel is sufficiently larger than the solid particle diameter so that the fluctuations in the fluid variables due to individual particles are smoothed out. These fluctuations are instead modelled by the particular particle drag term used, in our case the Stokes drag law. In other words, the AVNS equations assume a clear separation between the resolved length scales and the unresolved length scales associated with the drag force. In the simulations shown in Figure 3, the higher resolutions become comparable to the particle diameter, violating the main assumption of the AVNS equations and leading to an erroneous result.

In practice, this error should be corrected by using a drag law that incorporates the effect of the ratio between fluid resolution and particle diameter. Drag laws are generally a relationship between porosity and drag force for a given superficial velocity, and ideally they will be calculated using experimental or fully resolved simulation results where the representative length scale is equal to the resolution of the unresolved fluid simulation (i.e. a multiscale approach). If this is not feasible, then a more general drag term can be used (for example the Dallavalle and Di Felice terms in Eq. 23 and 24) provided that the fluid resolution is sufficiently low. From the data shown in Figure 4, an SPH particle separation of $2d$ (resulting in a smoothing length of $h = 3d$) results in an acceptable 4% error in the particle terminal velocity. Therefore this resolution will be used for the multiple particle sedimentation problem described in the next section.

VI. Multiple Particle Sedimentation

Most fluid-particle systems of interest will involve large numbers of particles, and therefore this test case involves the sedimentation of multiple particles through a water column. In this case, a layer of sedimenting particles is placed above a clear fluid region. Figure 5 shows the setup geometry. The fluid column is identical to the previous test case, but now the upper half of the column is occupied by an even distribution of DEM particles with a given porosity ϵ. The diameter and density of the particles is identical to the single particle simulation. The only other parameter change is that the particle Reynolds number is reduced to $Re_p = 0.01$ in order to slow down the

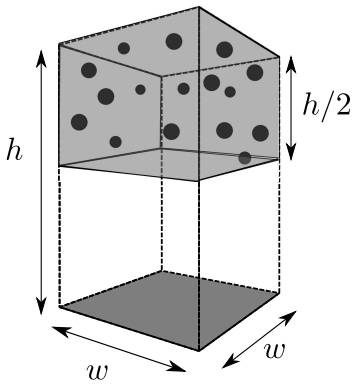

Fig. 5. Setup for multiple particle sedimentation test

terminal velocity of the particles and allow the instability more time to develop.

This setup is similar in nature to the classical Rayleigh-Taylor (RT) instability, where a dense fluid is accelerated (normally via gravity) into a less dense fluid. The combination of particles and fluid can be modelled as a two-fluid system with the upper "fluid" having an effective density of $\rho_c = \epsilon\rho_f + (1-\epsilon)\rho_s$, where ρ_f is the fluid density, and an effective viscosity μ_c. Using the hard sphere model proposed by Krieger [17], the effective viscosity can be estimated as

$$\frac{\mu_c}{\mu_f} = \left(\frac{\epsilon - \epsilon_{min}}{1-\epsilon_{min}}\right)^{-2.5(1-\epsilon_{min})} \tag{30}$$

where μ_f is the fluid viscosity and $\epsilon_{min} = 0.37$ is the porosity at the maximum packing density of the solid particles. We found that the growth rate of the RT instability for our chosen parameters was insensitive to changes in μ_c, therefore we conclude that the accurate estimation of μ_c is not essential for the analytical solution.

The two-fluid model of a Rayleigh-Taylor instability was derived in the authoritative text by Chandrasekhar [23]. The exponential growth rate $n(k)$ of a normal mode disturbance with wave number k at the interface between the two fluids (with zero surface tension) is characterised by the dispersion relation given by

$$\begin{aligned} &-\left[\frac{gk}{n^2}(\alpha_f - \alpha_c) + 1\right](\alpha_c q_f + \alpha_f q_c - k) - 4k\alpha_f\alpha_c \\ &+ \frac{4k^2}{n}(\alpha_f\nu_f - \alpha_c\nu_c)[\alpha_c q_f - \alpha_f q_c + k(\alpha_f - \alpha_c)] \\ &+ \frac{4k^3}{n^2}(\alpha_f\nu_f - \alpha_c\nu_c)^2(q_f - k)(q_c - k) = 0, \end{aligned} \tag{31}$$

where $\nu_{f,c} = \mu_{f,c}/\rho_{f,c}$, $\alpha_{f,c} = \rho_{f,c}/(\rho_f + \rho_c)$ and $q^2_{f,c} = k^2 + n/\nu_{f,c}$.

We generate an initial disturbance in the interface between the two "fluids" by adding a small perturbation to the vertical position of every DEM particle

$$-\frac{d}{4}(1 - \cos(k_x x_i))(1 - \cos(k_y y_i)), \tag{32}$$

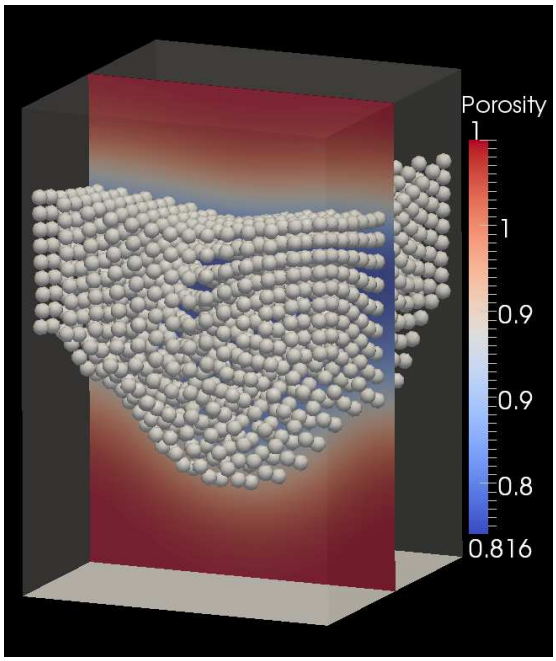

Fig. 6. Visualisation of the DEM particles for the multiple particle sedimentation test at $t = 12.51s$. Also shown is the porosity field at $x = 0$.

where $k_x = k_y = 2\pi$ and x_i and y_i are the x and y coordinates of the particle position. This yields a symmetric disturbance in the interface with a wave length equal to the box width w.

Figure 6 shows the positions of the DEM particles during the growth of the instability. This figure is taken at $t = 12.51s$, which is $2.51s$ after the release of the DEM particles from their initial positions. At this time there is a strong fluid circulation that is moving downward in the centre of the domain and upward at the edges. This causes the growth of the instability by increasing the sedimentation speed of the DEM particles near the centre while reducing or reversing the sedimentation of those particles near the outer boundaries of the domain.

The red crosses in Figure 7 show the vertical position of the lowest DEM particle. The vertical displacement of this point over time can be compared with the estimated growth rate for the RT instability as given by the two-fluid model in Eq. 31. Using the given parameters of the simulation and solving for the growth rate leads to $n = 1.18$. This compares well with the exponential fit to the SPH-DEM data, which results in an growth factor of $n = 1.3$. The growth rate of the simulated RT instability is slightly higher than expected, which is consistent with the data obtained from the single particle sedimentation test case. In that case we saw that the terminal velocity of the DEM particles is artificially increased (albeit slightly at this resolution) by the finite resolution of the fluid phase. This will lead to an increase in the growth rate of the RT instability, which is what we see in Figure 7.

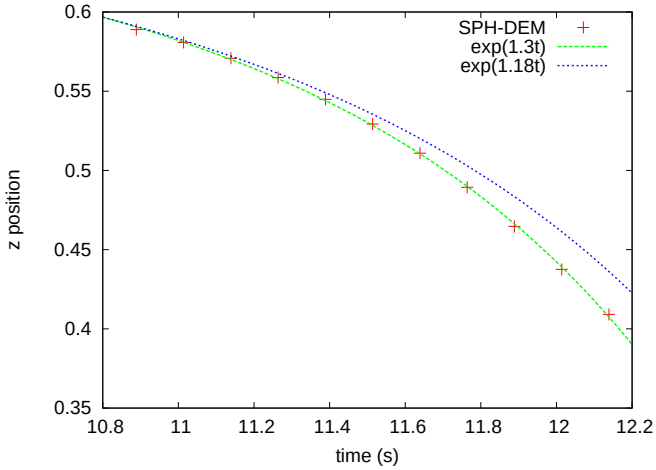

Fig. 7. Growth of Rayleigh-Taylor instability using the position of the lowest DEM particle. A fit of the data is shown as well as the expected growth rate using the two-fluid model.

VII. Conclusion

We have presented an SPH implementation of the locally averaged Navier Stokes equations and coupled this with a DEM model in order to provide a simulation tool for one or two-way coupled fluid-particle systems. One notable property of the resulting method is that it avoids the use of a mesh and is completely particle-based. It is therefore suitable for those applications where a mesh presents additional problems, for example, free surface flow or flow around complex, moving and/or intermeshed geometries.

The SPH-DEM formulation was applied to 3D single and multiple particle sedimentation problems and compared against analytical solutions. The method gave accurate results, provided that the resolution of the fluid phase is sufficiently larger than the DEM particle diameter. For these simulations it was found that an SPH smoothing length greater than $3d$ was enough to reduce the error to acceptable limits. However, a higher fluid resolution might be necessary for some applications, so future work in this area will focus on on characterising and correcting for the effects of a higher fluid resolution.

Acknowledgment

This work is supported by the PARDEM (www.pardem.eu) collaboration, which is a EU Funded Framework 7, Marie Curie Initial Training Network.

References

[1] Y. Zhu, P. Fox, and J. Morris, "A pore-scale numerical model for flow through porous media," *International journal for numerical and analytical methods in geomechanics*, vol. 23, no. 9, pp. 881–904, 1999.

[2] G. Pereira, M. Prakash, and P. Cleary, "SPH modelling of fluid at the grain level in a porous medium," *Applied Mathematical Modelling*, 2010.

[3] A. Potapov, "Liquid solid flows using smoothed particle hydrodynamics and the discrete element method," *Powder Technology*, vol. 116, no. 2-3, pp. 204–213, May 2001. [Online]. Available: http://dx.doi.org/10.1016/S0032-5910(00)00395-8

[4] Y. Tsuji, T. Kawaguchi, and T. Tanaka, "Discrete particle simulation of two-dimensional fluidized bed," *Powder Technology*, vol. 77, no. 1, pp. 79–87, October 1993. [Online]. Available: http://dx.doi.org/10.1016/0032-5910(93)85010-7

[5] B. Xu, "Numerical simulation of the gas solid flow in a fluidized bed by combining discrete particle method with computational fluid dynamics," *Chemical Engineering Science*, vol. 52, no. 16, pp. 2785–2809, August 1997. [Online]. Available: http://dx.doi.org/10.1016/S0009-2509(97)00081-X

[6] ——, "Numerical simulation of the gas solid flow in a bed with lateral gas blasting," *Powder Technology*, vol. 109, no. 1-3, pp. 13–26, April 2000. [Online]. Available: http://dx.doi.org/10.1016/S0032-5910(99)00223-5

[7] B. Hoomans, "Discrete particle simulation of bubble and slug formation in a two-dimensional gas-fluidised bed: A hard-sphere approach," *Chemical Engineering Science*, vol. 51, no. 1, pp. 99–118, January 1996. [Online]. Available: http://dx.doi.org/10.1016/0009-2509(95)00271-5

[8] B. Hoomans, J. Kuipers, and W. van Swaaij, "Granular dynamics simulation of segregation phenomena in bubbling gas-fluidised beds," *Powder Technology*, vol. 109, no. 1-3, pp. 41–48, April 2000. [Online]. Available: http://dx.doi.org/10.1016/S0032-5910(99)00225-9

[9] X. Li, X. Chu, and D. Sheng, "A saturated discrete particle model and characteristic-based SPH method in granular materials," *Int. J. Numer. Meth. Engng*, vol. 72, pp. 858–882, 2007.

[10] F. Jiang, M. Oliveira, and A. Sousa, "Mesoscale SPH modeling of fluid flow in isotropic porous media," *Computer Physics Communications*, vol. 176, no. 7, pp. 471–480, 2007.

[11] P. Cleary, M. Sinnott, and R. Morrison, "Prediction of slurry transport in SAG mills using SPH fluid flow in a dynamic DEM based porous media," *Minerals engineering*, vol. 19, no. 15, pp. 1517–1527, 2006.

[12] J. Fernandez, P. Cleary, M. Sinnott, and R. Morrison, "Using SPH one-way coupled to DEM to model wet industrial banana screens," *Minerals Engineering*, 2011.

[13] T. B. Anderson and R. Jackson, "Fluid mechanical description of fluidized beds. equations of motion," *Industrial & Engineering Chemistry Fundamentals*, vol. 6, no. 4, pp. 527–539, November 1967. [Online]. Available: http://dx.doi.org/10.1021/i160024a007

[14] N. Deen, M. Van Sint Annaland, M. Van Der Hoef, and J. Kuipers, "Review of discrete particle modeling of fluidized beds," *Chemical Engineering Science*, vol. 62, no. 1-2, pp. 28–44, January 2007. [Online]. Available: http://dx.doi.org/10.1016/j.ces.2006.08.014

[15] M. Van der Hoef, R. Beetstra, and J. Kuipers, "Lattice-Boltzmann simulations of low-Reynolds-number flow past mono-and bidisperse arrays of spheres: results for the permeability and drag force," *Journal of fluid mechanics*, vol. 528, no. -1, pp. 233–254, 2005.

[16] A. Einstein, "Berichtigung zu meiner arbeit: eine neue bestimmung der molekuldimensionen.," *Annalen der Physik*, vol. 34, pp. 591–592.

[17] I. Krieger, "A mechanism for non Newtonian flow in suspensions of rigid spheres," *Trans. Soc. Rheol.*, vol. 3, pp. 137–152, 1959.

[18] J. J. Monaghan, "SPH and Riemann Solvers," *Journal of Computational Physics*, vol. 136, pp. 298–307, Sep. 1997.

[19] D. Shepard, "A two dimensional function for irregularly spaced data." in *ACM National Conference*, 1968.

[20] J. Dallavalle, *Micromeritics: the technology of fine particles*. Pitman, New York, 1948.

[21] R. Di Felice, "The voidage function for fluid-particle interaction systems," *International Journal of Multiphase Flow*, vol. 20, no. 1, pp. 153–159, February 1994. [Online]. Available: http://dx.doi.org/10.1016/0301-9322(94)90011-6

[22] J. J. Monaghan, A. Kos, and N. Issa, "Fluid motion generated by impact," *Journal of waterway, port, coastal and ocean engineering*, vol. 129, pp. 250–259, 2003.

[23] S. Chandrasekhar, *Hydrodynamic and hydromagnetic stability*. Dover Pubns, 1961.